Remote Sensing for Planar Electrostatic Characterization using the Multi-Sphere Method

Heiko J.A. Engwerda*
Faculty of Aerospace Engineering
Delft University of Technology, Kluyverweg 1, 2629 HS, Delft, The Netherlands
Email: h.j.a.engwerda@student.tudelft.nl

Joseph Hughes
Aerospace Engineering Sciences Department
University of Colorado, ECEE 275, 431 UCB, 80309-0431, Boulder, CO, USA
Emails: Joseph.Hughes@Colorado.edu

Hanspeter Schaub
Aerospace Engineering Sciences Department
University of Colorado, ECEE 275, 431 UCB, 80309-0431, Boulder, CO, USA
Email: Hanspeter.Schaub@Colorado.edu

July 21, 2016

Summary
Applications like the Electrostatic Tractor (ET), remote sensing of space debris objects, or planetary science investigating asteroid charging, benefit from a touchless method to assess the electrostatic potential and charge distribution of another body. In the ET, accurate predictions of the force and torque between a passive space object and tug spacecraft are critical to ensure a robust closed loop control. This paper presents a novel, touchless method for determining both the voltage and a Multi-Sphere-Method (MSM) model which can be used to determine the charge distribution, force, and torque on a nearby space object. By means of potential probes, Remote Sensing for Electrostatic Characterization (RSEC) can be performed. Here the space tug shape and electrostatic potential is assumed to be known. The probes measure the departure from the expected potential field about the tug and determine an MSM model of the passive object's potential distribution. This paper outlines a method for estimating the voltage and charge distribution of a neighboring charged spacecraft undergoing a planar rotation given measurements of voltage over a full rotation. Assuming knowledge of the tug spacecraft's voltage and charge distribution, the rotation rate and distance to the debris, numerical simulation results illustrate that the constructed model of the debris can be characterized within a few percent error.

Keywords: *Electrostatic Tractor, Orbital Debris, Touchless Potential Sensing*

1 Introduction

Spacecraft formation flying is a popular topic within the aerospace community and offers many benefits. Swarms of satellites can provide a low cost solution to many space operations and allow for scientific studies that can not be performed with single spacecraft platforms.[1] Coulomb formation flying allows for small corrections within a satellite constellation without the use of propellant, but rather through the electrostatic force.[2] Between multiple charged bodies a Coulomb force exists which is inversely proportional to the square of the separation distance and product of the charges. Measuring the potential of the bodies is of importance to predict this force and the torques resulting from the charge distribution. Especially if one of the bodies is uncooperative, measurements of electric potential are crucial in maintaining operational safety. Over-prediction of the potentials may limit formation flying performance, while under-prediction can lead to collisions.[3] This paper presents a possible solution for estimating the potential and charge distribution of a nearby charged spacecraft with a known planar rotation rate using measurements of voltage in the vicinity of the debris. The force and torque on both bodies can be found from the voltage and charge distribution on the debris assuming the

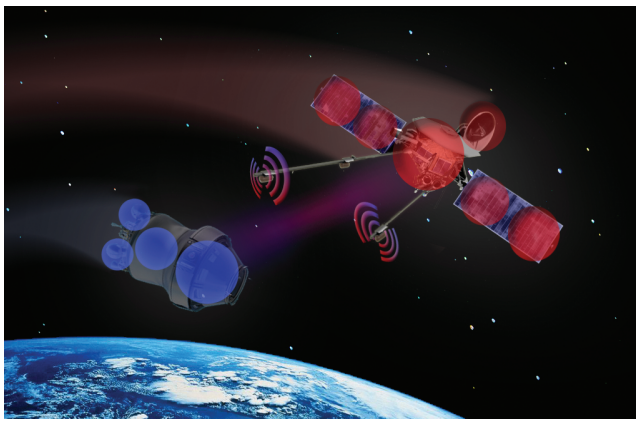

Figure 1: By means of potential probes, the electrostatic interaction between space objects can be characterized.

voltage and charge distribution are known for the tug.

One application of Coulomb formation flying with uncooperative spacecraft is the Electrostatic Tractor (ET), as proposed by Moorer and Schaub,[4,5] which applies the Coulomb interaction to reorbit space debris. Debris removal has been an increasingly popular topic in the recent years. The total amount of officially catalogued objects in Earth orbit exceeds 17,000, while only 23% of these objects is a payload.[6] Especially for regimes with many assets such as the Geostationary orbit (GEO), the development of the debris population is anxiously monitored since this orbit offers unique Earth monitoring and sensing possibilities. Of the total market of USD 20 billion, the majority of insured satellites resides in this orbit at 35,786 km altitude.[7] Since there is no passive clean-up mechanism, such as there is atmospheric drag in Low Earth Orbit, objects have to be manually removed. The most cost efficient option is to move the objects to a graveyard orbit, which is typically around 300 km above GEO.[8,9] At this altitude the decay time back to GEO exceeds 200 years, offering a (temporary) mitigation solution.[10] Over the years, several concepts have been proposed for moving the debris to such an orbit. The Ion Beam Shepherd proposed by Bombardelli and Pelaez[11] and the ET offer contact-less removal opportunities decreasing risks associated with debris removal, such as break-up events. Concepts such as nets, harpoons and grappling devices do introduce such risks as they require an established contact.[12] This paper focusses specifically on sensing potentials and estimating force and torque for the ET concept, but touchless electrostatic characterization has a broad applicability.

For example, there is interest in knowing the local potentials of asteroids and the moon. These measurements could help scientists better understand dust transport across the lunar surface[13,14] and asses risks encountered by spacecraft and astronauts during asteroid rendezvous missions.[15] It is of interest to measure these voltages without making electrical contact and thereby corrupting these measurements through discharge. It is also very difficult to make contact with a foreign body safely, as the Rosetta and Hayabusa missions have shown.[16] In order to apply the method described in this paper to such a mission, dielectric characteristics have to be incorporated in the model, which is beyond the scope of this paper.

In the ET concept, the tug irradiates the debris with electrons using an on-board electron gun. This causes the tug to become positively charged while the debris charges negatively. An electrostatic force and torque are felt on both craft, which can be used for touchless actuation.[17] Establishing the ET force is feasible in GEO due to the locally large Debye lengths of 200 meters and more.[18] The attractive Coulomb force resulting from the potential difference can be utilized to create a link between the bodies, while thrusting can be performed from the tug to move the multiple-body system to a graveyard orbit. As demonstrated by Albuja, inactive satellites can have very large rotation rates and depending on the symmetry of the body these rates evolve over time.[19] If the charge distribution on tug and debris is non-symmetric, the Coulomb force will generate a torque which can be used to detumble the debris in the span of a couple of days.[20]

The Coulomb force can be determined from the accelerations inferred from Light Detection and Ranging (LiDAR) measurements or other ranging methods over a long time. As discussed previously, Coulomb formation flying is inherently open-loop unstable and therefore estimation of the potential of debris in a feed-forward procedure is crucial. By means of measurements, the potential of the debris and thus the Coulomb force can be determined in real time. Possible sensing methods include placement of a probe on the debris, surface measurements, evaluation of charged particles[21,22] and contact-less electric field (E-field) or potential probing.[23] Because this paper focuses on remote and real-time sensing applications, only potential and E-field probes are considered.

By means of measuring the electric potential, Remote Sensing for Electrostatic Characterization (RSEC) of the debris can be performed. One or multiple probes are extended from the tug spacecraft using booms and register the electric potential field over time. This measurement is combined with the known debris spin rate and passed into a numerical solver to determine the potential of the debris and a Multi-Sphere Method (MSM) model for it. An artist's impression of this method can be found in Figure 1. This paper describes a touchless method for determining the voltage of a nearby space object and constructing an MSM model for it, which can be

used to predict the force and torque on the passive object. The sensitivity of the model with respect to input parameters and their errors is evaluated and a possible selection of probes is discussed.

2 Sensing Electric Potential

The RSEC model requires measurement of kilovolt potential at specific locations between tug and debris. Measuring potentials of spacecraft in space is a proven technology and can be performed even for kilovolt magnitudes. In its first year of operations, instruments on board of the Spacecraft Charging AT High Altitudes (SCATHA) satellite measured potentials as high as -14 kV during eclipse.[23] These measurements were obtained from plasma detectors, which consisted of electron- and ion detectors, as well as an electric field detector.

The most common methods to sense the electric potential in space is by means of Langmuir probes and emissive probes. Emissive probes are electrically heated which causes electron emission. This results in the probe reaching a floating potential and allows measurement of the plasma potential without requiring voltage sweeps.[24] Langmuir probes on the other hand do require voltage sweeps over a bias voltage. The measurements obtained from a sweep are related to the characteristic I-V curve and can be used to determine many plasma parameters.[25] Due to the high potential of the tug and sparse electron density in GEO, obtaining unambiguous measurements is expected to be difficult.

On Earth, electric field mills are commonly used to determine the electric field strength of thunderstorm clouds.[26] As E-fields are often more conveniently measured than potential fields in atmospheric conditions,[27] field mills are an appropriate choice for validation of the RSEC method in an atmospheric environment.

Most potential measurements that have been flown were designed to measure the ambient plasma potential or spacecraft potential with respect to the ambient (low potential) plasma. In this study, the spacecraft will be charged to tens of kV which requires adaptation of current available measurement methods. Around the tug, a large electron deficit exists, reducing the effectiveness of Langmuir probe measurements. Measurement of the space potential or electric field which results from being nearby a highly charged object is expected to be a difficult but possible task in space plasma. The authors are not aware of measurements currently being performed for mapping the spatial dependence of such high voltages (kV) or strong fields (kV/m).

Apart from the influence of the tug and debris on the sensors, there are a number of sources which may corrupt the measurements, such as interference of the booms and fluctuating space weather. Due to the high potential of the tug, not all of the emitted photo-electrons will be able to escape from the influence of the tug. When a probe is located in this photo-electron cloud, the measurements will be biased. In order to determine the radius $r_{\max}$ of this cloud, consider the following energy balance.

$$\underbrace{E_k + E_p}_{\text{Initial}} = \underbrace{E_k + E_p}_{\text{Final}} \tag{1a}$$

$$\frac{1}{2} m_e v_e^2 + q\frac{V_s R_s}{R_s} = q\frac{V_s R_s}{r_{\max}} \tag{1b}$$

In these equations, the electrons with mass m_e are emitted from the surface of a sphere of radius R_s and potential V_s with an electron-velocity v_e. The initial velocity (left hand side of Equation 1b) can be determined with Equation 2.

$$\frac{1}{2} m_e v_e^2 = q\phi_0 \tag{2}$$

Considering an average kinetic energy of 2 eV,[28] the velocity with which the photo-electrons are emitted is $v_e = 840$ km/s. Substituting values in Equation 1b gives a maximum distance travelled by the emitted electrons of 0.3 mm. Since close to the sphere the field deviates from that of a point source, the flat plate approximation as discussed by Grard may be more representative,[29] although application of this more realistic model is not expected to change the results drastically. The calculated value shows that the photo-electron cloud has a negligible influence on the probe measurements as long as they are placed on booms at distances on the order of multiple meters such as considered in the rest of this paper.

Another disturbance on the potential and electric field of two spheres is due to the presence of the electron beam. As an approximation, the beam can be represented as a line charge, for which the following equation holds.

$$V = \int \frac{k_c \mathrm{d}q}{r} = k_c \lambda \Psi \qquad k_c = \frac{1}{4\pi\epsilon_0} \tag{3}$$

The charge density λ can be determined from the kinetic energy of electrons in the beam (Equation 4b), where the integral over the beam length is represented by the parameter Ψ. The relation for Coulomb's constant k_c is given in the right hand side equation with ϵ_0 the permittivity of vacuum.

$$\lambda = \frac{I}{v_e} \tag{4a}$$

$$\frac{1}{2} m v_e^2 = eV \tag{4b}$$

Assuming an electron beam current of $I = 10$ mA and a potential V of 20 kV over a 10 m beam, the

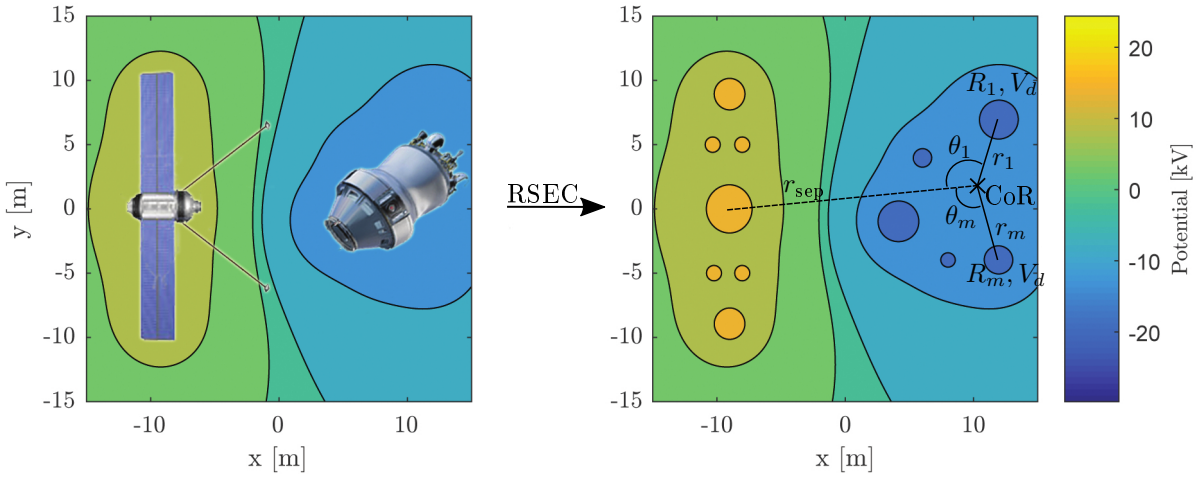

Figure 2: Angles and distances from the center of Rotation (CoR) towards spheres on the debris.

potential in the neighborhood of the beam is in the $0 - 8$ V regime. Such a beam current is 10 times higher than the minimum current required for charge transfer with a 4 m radius debris, as derived by Hogan et al.[28] Compared to the kilovolt potentials around the two bodies, this potential has minor significance and is neglected in the further analysis.

3 Electrostatic Characterization Model

The following section describes the RSEC model and the equations and assumptions required to construct this model. A graphical representation of the application of RSEC is given in Figure 2. The potential field resulting from the tug-debris system is measured by probes. The numerical RSEC model is then applied to find the parameters in an MSM model of the debris and it's voltage which best matches this measured potential field. This MSM model and potential are used to estimate the force and torque on the debris. This allows time-varying measurements of the voltage field to be used to estimate for the force and torque on both bodies faster-than-realtime.

3.1 Force, Torque and Potential Equations

Multiple methods have been developed which can be used to model the electrostatic characteristics of bodies in space. The easiest approximations is a 2-sphere model, as will be described in Section 5, but for small separation distances the tug and debris can not be accurately represented with single spheres. The non-homogeneous charge distribution and shape of the bodies affects not only the Coulomb force, but also introduces a torque on the bodies. Where the charge distribution can be very accurately predicted with Finite Element Method (FEM)[30] or the Method of Moments (MoM),[31] the computation time required often precludes real time simulations, in particular with FEM. An alternative is the MSM, which reduces computation time for a simple sphere-cylinder system from over an hour with FEM to a fraction of a second.[32]

If an MSM model of a tug consisting of n and debris of m-spheres is considered, the Coulomb force is written as a summation over all spheres.[33]

$$\boldsymbol{F}_c = k_c \sum_{j=1}^{m} \sum_{i=1}^{n} \frac{q_i q_j}{r_{i,j}^3} \boldsymbol{r}_{i,j} \tag{5}$$

In this equation the Debye shielding effect is neglected since the Debye length at GEO is much larger than the tug-debris separation distance ($\approx$ 200 m vs 20 m).[34] The torque on the debris is given by

$$\boldsymbol{T}_d = k_c \sum_{j=1}^{m} \sum_{i=1}^{n} \frac{q_i q_j}{r_{i,j}^3} \boldsymbol{r}_{i,j} \times \boldsymbol{r}_j \tag{6}$$

which is effectively the cross product of the forces and distance from the debris center of the rotation to the spheres. In order to compute the torque on the tug, r_j can be substituted by r_i.

Introducing multiple spheres in the MSM model also introduces a multiple of parameters which have to be solved for. In order to obtain as many unique equations as there are unknowns, electric potential measurements are taken over time for a rotating debris object. While the charge of all spheres varies over this tumbling motion, it is assumed that the electric potential of both bodies stays approximately constant during application of the tractor.[33]

Again considering a tug represented by n and debris of m-spheres, the charge on any of the total k spheres can be calculated from:

$$\begin{bmatrix} q_1 \\ q_2 \\ \vdots \\ q_k \end{bmatrix} = \frac{1}{k_c} \begin{bmatrix} 1/R_1 & 1/r_{2,1} & \dots & 1/r_{k,1} \\ 1/r_{1,2} & 1/R_2 & \dots & 1/r_{k,2} \\ \vdots & \vdots & \ddots & \vdots \\ 1/r_{1,k} & 1/r_{2,k} & \dots & 1/R_k \end{bmatrix}^{-1} \begin{bmatrix} \phi_1 \\ \phi_2 \\ \vdots \\ \phi_k \end{bmatrix} \tag{7}$$

The center matrix is known as the inverse capacitance matrix and it consists of the inverse self-capacitance C_t^{-1} of the tug and debris C_d^{-1} as well as the inverse mutual capacitance $C_{t,d}^{-1}$ and $C_{d,t}^{-1}$. In the MSM, inverse self capacitance is given analytically for a sphere, and the inverse mutual capacitance is found by treating both spheres as point charges:

$$\left[C^{-1}\right] = \begin{bmatrix} C_t^{-1} & C_{t,d}^{-1} \\ C_{d,t}^{-1} & C_d^{-1} \end{bmatrix} \qquad C_{d,t}^{-1} = C_{t,d}^{-1\,\mathrm{T}} \tag{8}$$

The inverse capacitance matrix describes the relationship between voltage and charge on both bodies at an instance of time. Since the position of the spheres is fixed within the bodies, the rotation rate determines the position at any instance of time. The only entries in the matrix that vary with this rate, and therefore have to be determined at each timestep, are $C_{t,d}^{-1}$ and its transpose. Pre-computing the other entries enables quick evaluation of this matrix at each time step. The inverse of the capacitance matrix can then be found from a block matrix inversion.[35] The potential curve that has to be matched against potential measurements follows from Equation 7. The potential at an instance of time at the probe location Φ_p is determined from the summation of all charges over their respective distance to the probe $r_{i,p}$.

$$\Phi_p = k_c \sum_{i=1}^{k} \frac{q_i}{r_{i,p}} \tag{9}$$

In this equation, the influence of the charge of the probe itself is neglected as this is expected to be calibrated by circuitry.

3.2 Obtaining the Best Fit MSM Model

Now consider the model given in the right-hand side of Figure 2. The location of the spheres on the debris is specified with respect to the center of rotation (CoR) which is at a constant and known distance from the tug center of mass. A constant rotation about the axis through the CoR, orthogonal to the plane of the spheres, is assumed to be determined by means of LiDAR. Alternatively this rotation rate could be estimated by waiting for the probe measurements to repeat. By doing so the potential measured by the probes at any time is a function of the state vector $\boldsymbol{x}$, which includes full planar MSM model and the voltage of the debris:

$$\boldsymbol{x} = [R_1, r_1, \theta_1, ...R_m, r_m, \theta_m, V_d] \tag{10}$$

Note that the characteristics of the tug are not defined in the state vector as they are assumed to be known a priori. These variables can be introduced to create a more general model, but for now they are assumed constant. Furthermore, the distance r_3 and rotation rate are not included as they are expected to be determined from LiDAR measurements. By using a numerical solver such as Matlab's *fmincon* function, the following cost function J is minimized in order to find the best fitting debris characterization.

$$J = \|\boldsymbol{\phi}_{\mathrm{P}}(\boldsymbol{x}, \boldsymbol{t}) - \boldsymbol{\phi}_{\mathrm{M}}(\boldsymbol{t})\| \tag{11}$$

Here $\boldsymbol{\phi}_{\mathrm{M}}$ and $\boldsymbol{\phi}_{\mathrm{P}}$ are vectors containing the measured and predicted probe potential at all measurement instances $\boldsymbol{t}$. In order to find a better solution, some non-linear inequality constraints are applied. As a first constraint, all of the spheres have to be located within a rectangular box of which the contours have a 10 cm offset from most outward surface of the truth model. The second constraint makes sure that all sphere locations are unique by calculating the distance between spheres and requiring a minimal separation of 50 cm. This constraint is enforced because closely placed spheres make the inverse capacitance matrix difficult to invert numerically. Additionally, upper and lower bounds are applied on the state vector to restrict the radii of the spheres and their potential, such that no non-zero radii and potentials exist. The initial state vector is constructed as a spiral of spheres such that no sphere locations are identical, and all have a -15 kV potential.

The obtained solution state vector describes the electrostatic characteristics of the debris. After obtaining this characterization, potential measurements can be used to determine the force and torque at any instance of time, assuming the rotation rate and potential stay constant. As the potential of the tug and debris is expected to vary with the space weather, the orbit does play a role. From an analysis performed by Denton et al, it follows that except for a few hours after local midnight, the ambient plasma temperature and density varies over the scale of hours.[18] Considering that force and torque estimates could be made multiple times per minute, assuming the potential to be constant is deemed a good assumption.

4 Numerical Simulation Example

In the following section, the results from an example numerical simulation are given to demonstrate the applicability and performance of the RSEC method. Furthermore, a parameter sweep and sensitivity study are performed to examine the robustness of the method.

4.1 Set-up and RSEC Results

The simulation is performed for a truth model consisting of 18 spheres on the debris and 4 spheres on the tug. By means of the RSEC method, the debris is approximated with a solution consisting of only 10 spheres. Two probes acquire the potential

Table 1: Truth model input parameters.

Tug Potential: +20 kV Debris Potential: -20 kV		
Tug		
Sphere	Location (x y) [m]	Radius [cm]
1	(-5 1);	10
2	(-5 -1);	20
3	(-7 1);	5
4	(-7 -1)	3
Debris		
Sphere	Location (x y) [m]	Radius [cm]
1	(5 1)	10
2	(5 -1)	8
3	(7 1)	7
4	(7 -1)	4
5	(8 0)	3
6	(6 0)	7
7	(4 0)	9
8	(8 1)	2
9	(8 -1)	3
10	(6 1)	5
11	(6 -1)	4
12	(4 1)	9
13	(4 -1)	8
14	(6 2)	4
15	(6 3)	5
16	(6 4)	1
17	(5 -2)	4
18	(9 0)	2
Probes		
Probe	Location (x y) [m]	Measurements
1	(-1 5)	15
2	(-1 -5)	15

measurements, being located approximately 5 m from the tug under a 45° angle with the debris. In order to obtain the measured potential curves, 15 measurements equally distributed over a full rotation of the debris are used. An overview of these parameters can be found in Table 1.

The potential measured by the probes in both the truth (18 sphere) and solution (10 sphere) model are plotted over rotation angle in Figure 3. From these curves, it can be concluded that the numerical solver is able to quite accurately determine the potential curve of the solution. The error in potential between truth and solution is at most 0.01%. The corresponding potential field of truth and solution can be found in Figures 4 and 5 respectively.

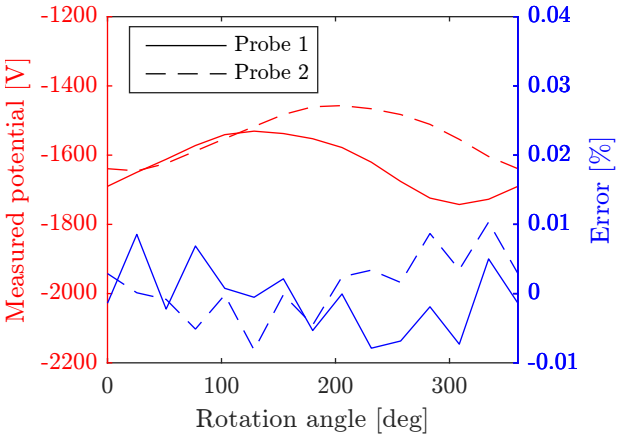

Figure 3: Measured potential by two probes, potential of the solution, and difference between the two.

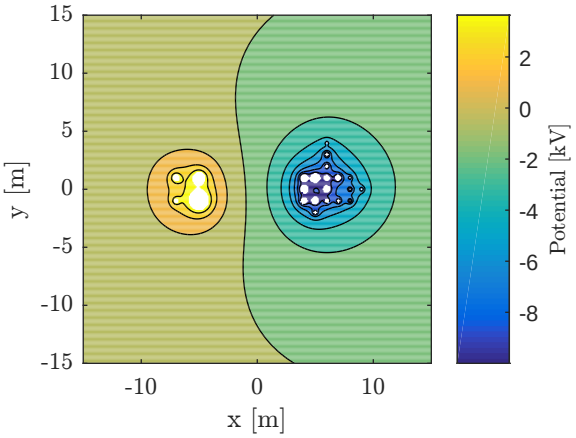

Figure 4: Surface plot showing the 2D potential field of the truth model tug-debris system.

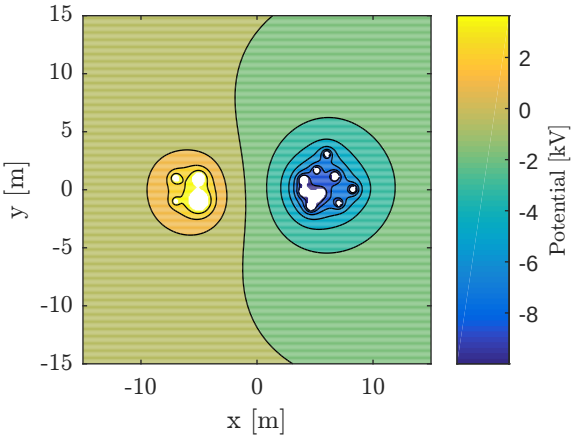

Figure 5: Surface plot showing the 2D potential field of the solution model tug-debris system.

From these figures, it can be noticed that the potential field approximates a dipole field for larger separations. Moreover, while the field internal to the debris deviates significantly from the truth, the external field is accurately represented. Since the force and torque on both bodies is of interest and not the field structure internal of the debris, this deviation can be neglected. In order to determine the force and toque, Equations 5 and 6 are applied. Rotating the debris over time yields the distribution for force and torque over debris rotation angle, as give in Figures 6 and 7 respectively.

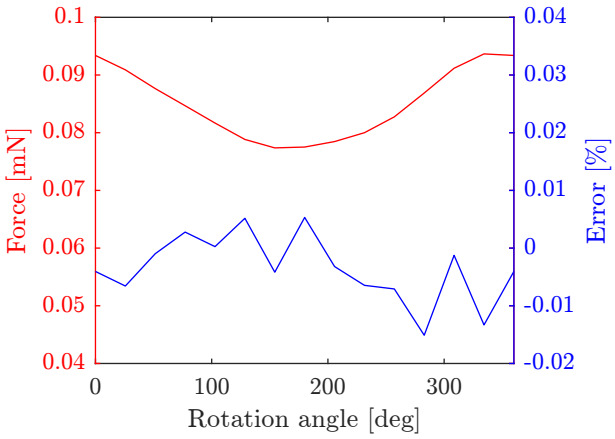

Figure 6: Force of the solution model as well as its error with respect to the truth, over debris rotation angles.

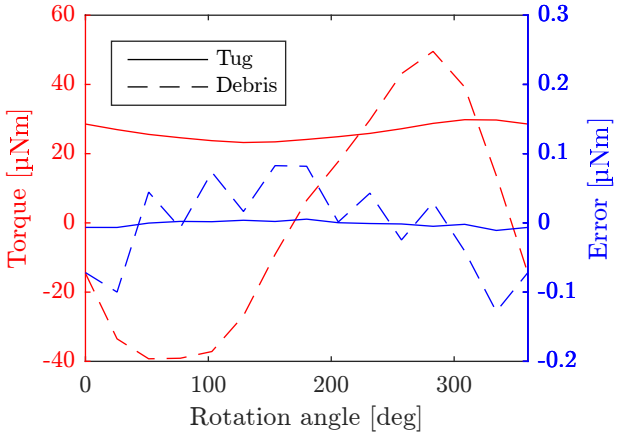

Figure 7: Torque on tug and debris of the solution model as well as its error with respect to the truth, over debris rotation angles.

From these figures, it can be seen that even though the spheres are placed at significantly different positions than in the truth model, the resulting force and torque are still accurate below 1%. The range of error in force is comparable to that of the measured potential and even though the torque on the debris has the largest error, it is still quite accurate.

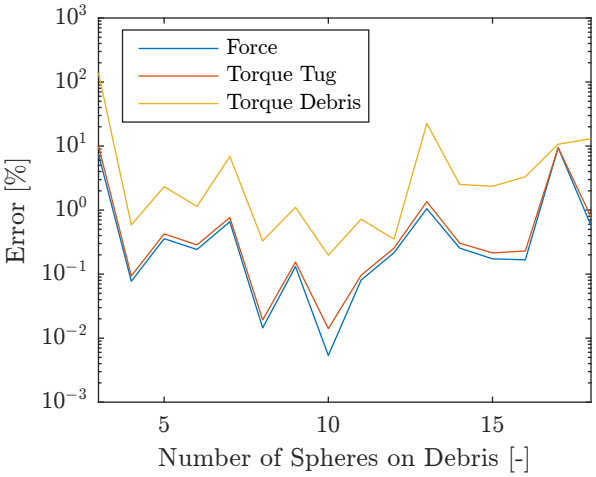

Figure 8: Error in force versus amount of spheres in the debris model.

4.2 Performance Sweep over Parameters

In order to show the influence of input parameters on the accuracy of the electrostatic characterization, a variation of parameters is performed. The same model is used as in the example set up in the previous section. Instead of applying a fixed number of 10 spheres to represent the debris, this number is varied. As can be seen in Figure 8, a solution represented by too few spheres will introduce large errors in the solution. A cause for this error is symmetric sphere placement, which can be alleviated by adding another probe such that two potential curves have to matched instead of just one. Furthermore it is deduced from Figure 8 that even though the truth model consists of a large number of spheres, the solution will not be optimal with the same number of spheres. This may be because the optimizer has too many free parameters. A representation by as little as 4 spheres already generates a solution that models the system very well.

The fields and their angular dependance are smaller if the two spacecraft are farther apart. Their separation was also varied to see how performance was affected. Refering to Figure 9, it can be concluded that the influence of this distance on the error in force and torque is negligible. The error appears to be a function of the geometry of the example set up and the ability of the solver to find an optimal state vector. However, the accuracy of LiDAR and probes may degrade due to the increased distance and smaller field strength.

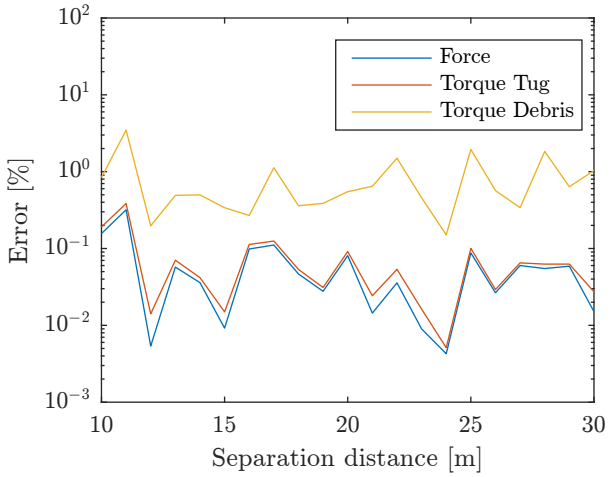

Figure 9: Error in force versus separation distance between tug and debris center of mass.

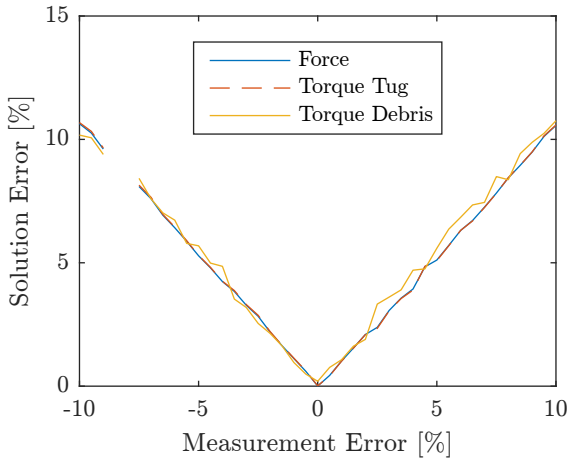

Figure 11: Error in the solution in terms of force and torque due to an error in the potential measurements.

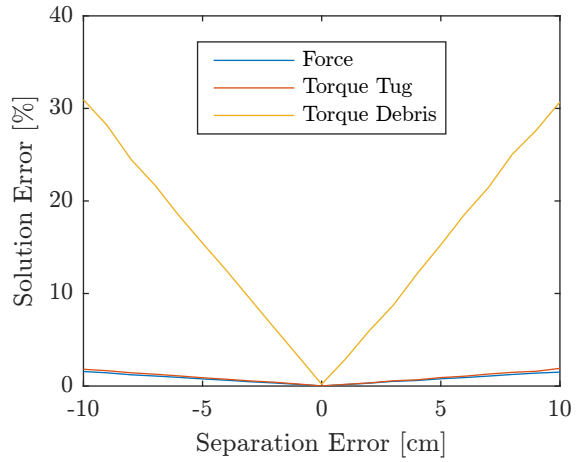

Figure 10: Error in the solution in terms of force and torque due to an error in the measured separation distance.

4.3 Sensitivity with respect to Separation and Measurement Error

One of the assumptions in the described model is that the separation distance between tug and center of rotation of the debris is known. In order to see what an error in measurements of this distance does to the accuracy of the results, a sensitivity analysis is performed.

Figure 10 is acquired with the assumption that LiDAR will introduce measurement errors in the *cm* range. Although the force between tug and debris is still accurately represented by the solution, the torque on the debris will deviate rapidly from the truth model. In order to stay in the percent error range, millimetre accuracy is therefore required from LiDAR. In application of LiDAR, distance is measured from the sensor towards a reflecting surface. Since the separation distance is defined from center of the tug to the center of rotation of the debris, this discrepancy has to be accounted for.

Assuming that the separation distance is perfectly determined, the error in the solution will still be non-zero due to errors in the probe measurements. In Chapter 2, it is determined that measurements near the electron beam will deviate by less than 10 V. Adding the interference of booms and space weather to this measurement error is expected to result in a percent error scale. By running the RSEC solver with a percent error in the measurements, Figure 11 is obtained.

The omitted data in Figure 11 corresponds to outliers due to the solver's inability to converge to a proper solution. In the figure, a clear trend can be distinguished, showing an almost 1-on-1 linear relation between measurement percent error and solution percent error for both force and torque.

5 2-Sphere Model for Probe Placement

By reducing the RSEC model to a 2-sphere model, the sensitivity with respect to probe placement can be analytically evaluated. It is demonstrated that the tug-debris system approximates a dipole field for larger separation distances which indicates that the results of the 2-sphere model may also hold for multi-sphere models of simple spacecraft geometries. Such a model could also be used for validating Earth-based experiments. Since E-field mills are expected to provide the most accurate measurements in atmospheric conditions, the analytic 2-sphere model is derived using E-field measurements.

5.1 Force Model

For a first order approximation of the force between tug and debris, two spherical bodies are considered. There

is no torque between these two spheres in this model, and if Debye shielding is neglected, the Coulomb force between a charge q_T on the tug and q_D on the debris can be written in vector form as

$$\boldsymbol{F}_c = k_c \frac{q_T q_D}{r^3} \boldsymbol{r} \tag{12}$$

where r is the separation distance. Appropriate separation distance is selected based on the required force for re-orbiting as well as induced charging effects and safety during close proximity formation flying. It is shown by Schaub et al, that the mN Coulomb force obtained at $15 - 20m$ separation and kV potentials, results in reorbiting times of $2 - 4$ months to a graveyard orbit.[36]

5.2 2-Sphere Model

An illustration of deriving the Coulomb force acting between two charged objects from measurements is be given below. Consider the case as represented in Figure 12

The E-field measured by the probes can be written as

$$E_{1x} = k_c \frac{q_t}{r_1^2} + \sin\alpha_1 k_c \frac{q_d}{r_4^2} \tag{13a}$$

$$E_{1y} = \cos\alpha_1 k_c \frac{q_d}{r_4^2} \tag{13b}$$

where $\alpha_1 = f(\theta_1, r_1, r_3)$, $r_4 = f(\theta_1, r_1, r_3)$. Rewriting Equations 13 yields expressions for the charge on tug and debris. Substitution of these expressions into Equation 12 results in the force between tug and debris:

$$F = \left(E_{1y}\frac{r_1 r_4}{r_3}\right)^2 \frac{\sec\alpha_1}{k_c}\left(\frac{E_{1x}}{E_{1y}} - \tan\alpha_1\right) \tag{14}$$

By measuring the location of the debris (θ_1 and r_3), the Coulomb force can be determined. In space applications with an absence of LiDAR, an additional probe (see Figure 12) can be utilized to determine the angle θ_1 and separation distance r_3.

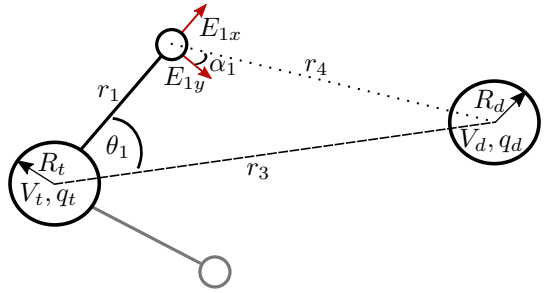

Figure 12: Schematic of angles and distances between spheres and probes.

5.3 Optimal Probe Placement

In order to determine what the best location for the probes with respect to tug and debris is, the sensitivity of force with respect to the E-field measurements is derived for the simple 2-sphere model. Taking the norm of the partial derivatives of Equation 14 with respect to E_{1x} and E_{1y} gives the following equation.

$$\left\|\frac{\mathrm{d}F}{\mathrm{d}E}\right\| = \frac{\sec\alpha_1}{k_c}\left(\frac{r_1 r_4}{r_3}\right)^2 \sqrt{E_{1y}^2 + \left(E_{1x} - 2E_{1y}\tan\alpha_1\right)^2} \tag{15}$$

This is the sensitivity of the force estimate to a spurious electric field measurement. To obtain a force estimate that is robust to sensor error, this value should be small. As a representative study of this equation, a tug and debris with ±20 kV potential and radii of 3 m are selected. For this case, the logarithm of Equation 15 is displayed in the middle of Figure 13. By setting the potential of tug or debris to ±10 kV and 2 m respectively, the outer figures are obtained.

The result from Figure 13 is rather intuitive. When the potential of the tug is larger in magnitude than that of the debris, better force predictions result from placing the probe closer to the debris. Vice versa, the probe should be located closer to the tug when its potential is lower in magnitude than that of the debris. Due to the measurements orthogonal to the tug field E_{1y}, the probe should not be located directly in between the two bodies since the field in y-direction will be zero. Even more so, the tractor beam will be located along this separation vector meaning that the measurements will be corrupted. Lastly, around the zero-potential gradient (see Figure 5), the influence of small external fields will become significant and measurements could result in corrupted data. More in-depth study of probe placement is therefore envisioned.

6 Conclusion and Recommendations

Assuming knowledge of the tug potential, the center-to-center separation between tug and debris, and measurements of space potential or electric field in the vicinity of the craft, the voltage and an MSM model of the debris can be found using the method outlined here. This is done by constructing a predicted curve of potential vs. time for each probe and comparing it to the measured curve. Although special attention is paid to the ET, the method proposed could be used for electrostatic characterization of objects of interest such as asteroids. The potential field of this solution distribution matches the truth MSM model within percentage error. Even more so, the force and torque are also within percentage range. By performing a variation of parameters and sensitivity analysis, it

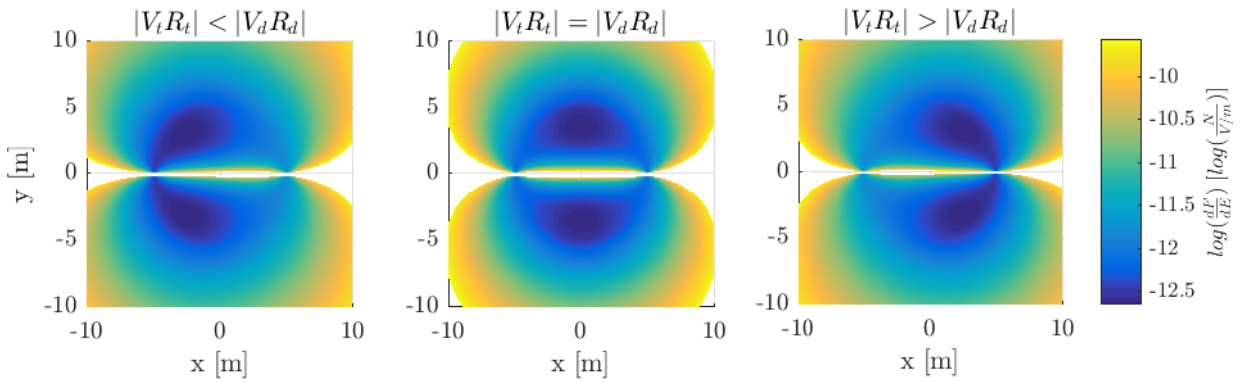

Figure 13: Surface plots showing the derivative of force with respect to E-field measurements for a tug located at (-5,0) and debris at (5,0) with $\pm 20kV$ potentials.

can be found that only a small number of spheres is required to accurately characterize the electrostatic behaviour of the debris. By placing the probes closest to the body with least potential magnitude, the best results are obtained. This is under the conditions that the measured separation distance has errors in the millimetre range and external influences such as the photo-electron cloud and potential field due to the tractor beam are negligible.

Future validation of these results is envisioned by using a field-mill to measure the electric field between spherical probes in a test-bed. The described 2-sphere model can be used for this validation. Furthermore, the planar model described in this paper does not account for 3D satellite dimensions and tumbling motion. The next step in developing the RSEC model therefore includes implication of general 3D shapes and dynamics. This model can be optimized by using appropriate estimators, such as a Kalman filter in place of Matlab's *fmincon* solver. Using an estimator is expected to improve the accuracy of the results and offer better feed-forward estimations.

References

[1] Bristow, J., Folta, D., and Hartman, K. A formation flying technology vision. *AIAA Paper* **5194**, 19–21 (2000).

[2] Vasavada, H. and Schaub, H. Analytic solutions for equal mass four-craft static coulomb formation. *The Journal of the Astronautical Sciences* **56**(1), 17–40 (2008).

[3] Hogan, E. and Schaub, H. Relative motion control for two-spacecraft electrostatic orbit corrections. *Journal of Guidance, Control, and Dynamics* **36**(1), 240–249 (2012).

[4] Schaub, H. and Moorer, D. F. Geosynchronous large debris reorbiter: Challenges and prospects. *The Journal of the Astronautical Sciences* **59**(1–2), 161–176 (2014).

[5] Moorer, D. and Schaub, H. Electrostatic spacecraft reorbiter. US Patent 8,205,838 B2, 06 (2012).

[6] National Aeronautics and Space Administration (NASA). Satellite box score. *Orbital Debris Quarterly News* **20**(1-2), 12–14 (2016).

[7] Chrystal, P., McKnight, D., Meredith, P. L., Schmidt, J., Fok, M., and Wetton, C. Space debris: On collision course for insurers? Technical report, Swiss Reinsurance Company Ltd, Zürich, Switzerland, March (2011).

[8] Johnson, N. Protecting the geo environment: policies and practices. *Space Policy* **15**(3), 127–135 (1999).

[9] Inter-Agency Space Debris Coordination Committee (IADC). IADC space debris mitigation guidelines. Technical Report IADC-02-01, Inter-Agency Space Debris Coordination Committee, September (2007).

[10] Ariafar, S. and Jehn, R. Long-term evolution of retired geostationary satellites. *4th European Conference on Space Debris* **587**, 681 (2005).

[11] Bombardelli, C. and Pelaez, J. Ion beam shepherd for contactless space debris removal. *Journal of guidance, control, and dynamics* **34**(3), 916–920 (2011).

[12] Kaplan, M., Boone, B., Brown, R., Criss, T., and Tunstel, E. Engineering issues for all major modes of in situ space debris capture. In *Proceedings of the AIAA SPACE 2010 Conference & Exposition*. (, Anaheim, 2010).

[13] Farrell, W., Stubbs, T., Vondrak, R., Delory, G., and Halekas, J. Complex electric fields near the lunar terminator: The near-suface wake and accelerated dust. *Geophysical Research Letters* **34**(14) (2007).

[14] Hartzell, C. M. *The dynamics of near-surface dust on airless bodies.* PhD thesis, University of Colorado Boulder, (2012).

[15] Jackson, T., Zimmerman, M., and Farrell, W. Concerning the charging of an exploration craft on and near a small asteroid. In *45th Lunar and Planetary Science Conference*, (2014).

[16] Ulamec, S. and Biele, J. Surface elements and landing strategies for small bodies missions–philae and beyond. *Advances in Space Research* **44**(7), 847–858 (2009).

[17] Schaub, H. and Jasper, L. Circular orbit radius control using electrostatic actuation for 2-craft configurations. *Advances in the Astronautical Sciences* **142**, 681 (2011).

[18] Denton, M., Thomsen, M., Korth, H., Lynch, S., Zhang, J., and Liemohn, M. Bulk plasma properties at geosynchronous orbit. *Journal of Geophysical Research: Space Physics* **110**(A7) (2005).

[19] Albuja, A. A. *Rotational Dynamics of Inactive Satellites as a Result of the YORP Effect.* PhD thesis, University of Colorado Boulder, (2015).

[20] Bennett, T. and Schaub, H. Touchless electrostatic three-dimensional detumbling of large geo debris. In *AAS/AIAA Spaceflight Mechanics Meeting* (, Santa Fe, New Mexico, 2014).

[21] Mizera, P., Fennell, J., Croley, D., and Gorney, D. Charged particle distributions and electric field measurements from s3-3. *Journal of Geophysical Research: Space Physics* **86**(A9), 7566–7576 (1981).

[22] Pfaff, R., Borovsky, J., and Young, D. *Measurement Techniques in Space Plasmas: Particles.* American Geophysical Union, Washington, DC., (1998).

[23] Mullen, E. and Gussenhoven, M. Scatha survey of high-level spacecraft charging in sunlight. *Journal of Geophysical Research* **91**(A2), 1474–1490 (1986).

[24] Kemp, R. and Sellen Jr, J. Plasma potential measurements by electron emissive probes. *Review of Scientific Instruments* **37**(4), 455–461 (1966).

[25] Boyd, T. and Sanderson, J. *The physics of plasmas.* Cambridge University Press, Cambridge, (2003).

[26] Chubb, J. Two new designs of 'field mill' type fieldmeters not requiring earthing of rotating chopper. *IEEE Transactions on Industry Applications* **26**(6), 1178–1181 (1990).

[27] Secker, P. and Chubb, J. Instrumentation for electrostatic measurements. *Journal of electrostatics* **16**(1), 1–19 (1984).

[28] Hogan, E. and Schaub, H. Impacts of tug and debris sizes on electrostatic tractor charging performance. *Advances in Space Research* **55**(2), 630–638 (2015).

[29] Grard, R. Properties of the satellite photoelectron sheath derived from photoemission laboratory measurements. *Journal of Geophysical Research* **78**(16), 2885–2906 (1973).

[30] Jin, J. *The finite element method in electromagnetics.* John Wiley & Sons, Hoboken, NJ., (2014).

[31] Gibson, W. *The method of moments in electromagnetics.* CRC Press, Boca Raton, FL., (2014).

[32] Stevenson, D. and Schaub, H. Optimization of sphere population for electrostatic multi-sphere method. *IEEE Transactions on Plasma Science* **41**(12), 3526–3535 (2013).

[33] Stevenson, D. and Schaub, H. Multi-sphere method for modeling electrostatic forces and torques. *Advances in Space Research* **51**(1), 10–20 Jan. (2013).

[34] Seubert, C., Stiles, L., and Schaub, H. Effective coulomb force modeling for spacecraft in earth orbit plasmas. *Advances in Space Research* **54**(2), 209–220 (2014).

[35] Jo, S., Kim, S., and Park, T. Equally constrained affine projection algorithm. *Conference Record of the Thirty-Eighth Asilomar Conference on Signals, Systems and Computers* **1**, 955–959 (2004).

[36] Schaub, H. and Sternovsky, Z. Active space debris charging for contactless electrostatic disposal maneuvers. *Advances in Space Research* **53**(1), 110–118 (2014).